Applied Catalysis B: Environmental 225 (2018) 207–217

Contents lists available at ScienceDirect

Applied Catalysis B: Environmental

journal homepage: www.elsevier.com/locate/apcatb

Design of catalytic carbon nanotube-based reactor for water denitration – The impact of active metal confinement

Sanja Panić[a,*], Ákos Kukovecz[b], Goran Boskovic[a]

[a] University of Novi Sad, Faculty of Technology, Bulevar cara Lazara 1, 21000, Novi Sad, Serbia
[b] University of Szeged, Department of Applied and Environmental Chemistry, Rerrich Bela ter 1, H-6720, Szeged, Hungary

ARTICLE INFO

Keywords:
Carbon nanotubes cutting
Pd-Cu nanoparticles decoration
Carbon nanotube-based reactor
Confinement effect
Catalytic denitration

ABSTRACT

The catalytic reduction of nitrate to N_2 represents the efficient water remediation technique in terms of the achieved nitrate depletion, but still with a main drawback – the production of ammonia as the undesired product. Therefore, efforts are undertaken to solve the problem, in terms of both reactor and catalyst design. Usage of internal cavities of carbon nanotubes (CNTs) may be a solution, both as a catalyst support and chemical nanoreactor. The aim of this work was to examine the activity and selectivity of Pd-Cu active phase located inside the carbon nanotubes – the confinement effect. Due to more accurate analysis of this effect, catalytic behavior of the metal nanoparticles deposited on the CNT exterior walls was also tested. Positioning of the active metal phase, *i.e.* exclusively inside or outside the CNTs, was promoted by previous CNTs cutting (*via* catalytic oxidation) and using solvents of different surface tension. The results of catalytic tests revealed the hindering effect of confined metal nanoparticles, while the externally deposited ones can be portrayed by superior performances in terms of both their activity and selectivity. The unexpected result was explained by a negative impact of confined particles due to their electron deficiency, as well as their size determining the second step of denitration reaction as a structure sensitive one.

1. Introduction

Since their discovery in 1991, the unique tubular morphology of carbon nanotubes (CNTs) represents a great research challenge for many scientists over the world. The possibility of using the inner cavity of CNTs for depositing various materials is still under extensive exploration. The well-defined channels of nanotubes restrict the size of encapsulated materials creating a reactor with nanometer or even subnanometer particle sizes. The early developed synthesis techniques were successfully applied for complete filling of CNTs and production of metallic nanowires [1]. Later, the further development of these methods enabled the selective confinement of a large range of materials in the form of discrete nanoparticles. The confinement phenomenon has been intensively examined in the field of catalysis offering a lot of possibilities for designing new catalysts and/or nanoreactors based on CNTs. It has been evoked in the literature that due to the curvature of CNT walls, the π electron density is shifted from the concave inner to the convex outer surface, which affects the electronic structure of the metal particle sitting in the tube interior, consequently changing the activity and selectivity of the corresponding catalyst [2]. So far, a broad range of catalytic chemical reactions have been conducted in order to study the possibility of tailoring the catalyst properties and performances by nanoscale confinement, eventually leading to different reaction pathways and distribution of products. Most of the obtained results have confirmed that metal confinement inside CNTs results in enhanced catalytic behavior compared to the tubes with particles dispersed on their exterior surface [3–5]. This might be partially assigned to the lower rate of particle agglomeration resulting in the prevention of catalyst deactivation [6]. However, negligible or even hindering impact of inner position of the metal particles was observed in a few reports as well [7–9]. These results are also considered very important from the perspective of further catalyst design and the development of new nanoreactor methodologies.

Nowadays, among all literature reported filling techniques, wet chemistry methods seem to be the most applicable due to their simplicity and versatility [10,11]. Many metals and metal oxides can be deposited inside the CNTs from inorganic or organic solutions of their precursors by capillary forces. Since the filling extent depends on the surface tension of the liquid and the CNT walls wettability, the position of nanoparticles can be additionally tailored by choosing the appropriate solvent [11]. However, the homogeneous distribution of particles exclusively on interior or exterior surface of the tubes is still difficult to

* Corresponding author.
E-mail address: sanjar@tf.uns.ac.rs (S. Panić).

https://doi.org/10.1016/j.apcatb.2017.11.078
Received 17 July 2017; Received in revised form 10 November 2017; Accepted 28 November 2017
Available online 01 December 2017

achieve, especially with CNTs with diameters less than 10 nm [12]. Consequently, in order to improve the selectivity of the process, several strategies have been developed. The most common ones imply the CNT cutting [13], resulting in enhanced particles deposition within CNT interior due to the minimization of mass transport restrictions. Another approach might be asymmetric modification (functionalization) of the concave and convex tube surfaces [14].

The water denitration is of great environmental significance since the pollution of underground water, an important source of potable water, has become a widespread concern in many countries due to excessive use of chemical fertilizers. High level of nitrate in drinking water is known to be a potential risk to human health causing various diseases. Among the current available remediation processes, catalytic denitration has an advantage compared to the other methods being an eco-friendly and economically viable process [15]. However, the main drawback of this process is the production of ammonia as the undesired product. Up to now, numerous bimetallic catalytic systems comprising of a precious metal (Pd, Pt, Rh) and a promoting transition metal (Cu, Ni, Fe, Sn, In) have been widely tested in order to establish the catalyst with enhanced performances. Among them, the Pd-Cu active phase has been emphasized in many reports as the most effective system, but still inadequate in terms of selectivity to nitrogen [16,17]. According to the accepted mechanism, bimetallic Pd-based entities are essential for the conversion of nitrate to nitrite, while the further nitrite reduction occurs solely on Pd monometallic sites [18,19].

The exploration of the catalysts in the form of carbon nanoreactors has been mainly focused on various hydrogenation and oxidation reactions. This paper is the first one dealing with the CNT-based catalyst confinement effect in water denitration reaction. The main idea behind the confinement effect is the possibility of lenient reaction conditions practice and consequent achievement of higher selectivity. In addition, the size of active metal particles in a carbon nanotube-based reactor offers advanced catalytic activity due to higher active sites dispersion. The last, but not the least, correlation of denitration reaction selectivity and active metal particle size (pointed by the tube channels confinement effect) might be important. Namely, there are few papers dealing with denitration reaction selectivity focusing on its second step structure sensitivity [20–22], however the results are diverse depending on applied active metals (Pd or Pt). Therefore, the activity and selectivity of Pd-Cu active phase placed inside the carbon nanotubes were examined in this paper, with special emphasis on nitrogen selectivity. In order to favor the filling of the tube interior, the original long multi-walled carbon nanotubes were catalytically shortened (and consequently opened) prior to the metal deposition. The confinement effect study implied a control sample test, assuming the same metal nanoparticles dispersed entirely on external surface of the same carbon nanotubes.

2. Experimental

2.1. Synthesis and functionalization of multi-walled carbon nanotubes (MWCNTs)

MWCNTs synthesis was carried out for one hour in a flow of ethylene/nitrogen mixture (1:1) at 700 °C, using an *in situ* pre-reduced 5% Fe-Co/Al_2O_3 catalyst in a home-made reactor setup that was described earlier [23,24]. The obtained raw material was boiled under reflux for 6 h in diluted NaOH and concentrated HNO_3 solutions, respectively, in order to remove the catalyst remains and functionalize the MWCNT surface. The resultant sample was collected on a filter and rinsed with distilled water until a pH neutral followed by drying at 110 °C for 24 h. The obtained long nanotubes, labeled as LMWCNTs (L = long), have been proved as free from any catalyst remains [24].

2.2. Oxidative cutting of MWCNTs

The catalytic oxidation of previously prepared LMWCNT sample was performed in the presence of Ag as a catalyst, selected based on the well-known fact that it catalyses the oxidation of hydrocarbon compounds [25]. Among the other transition metals (Au, Cu, *etc.*) with the same ability, Ag is the most efficient one [26,27]. The catalytic role of Ag nanoparticles in oxidative cutting has also been confirmed by the reduction of CNT oxidation temperature [28].

The nanotube sample was ultrasonically impregnated with aqueous $AgNO_3$ (Centrohem, Serbia) solution in order to achieve the nominal 5 wt.% Ag. The obtained suspension was further treated for 3 h at 40 °C followed by vacuum evaporation of the excess solvent. The solid residue was dried in an oven at 120 °C for 24 h. Silver nanoparticles were obtained by decomposition of $AgNO_3$ heated in an oven at 2 °C/min up to 300 °C in N_2 flow and maintained at the final temperature for the next 3 h. The catalytic oxidation of CNTs was carried out by switching the gas stream from N_2 to air and subsequently cooling the sample rapidly after 90 min of reaction time. The used Ag nanoparticles were removed from nanotubes by additional ultrasonic treatment in 2 M HNO_3 for 3 h at 40 °C. After filtration, washing and drying, the prepared nanotube sample was labeled as SMWCNTs (S = short).

2.3. Synthesis of Pd-Cu catalysts for water denitration

The SMWCNT sample was used for the synthesis of two bimetallic 2% Pd – 1% Cu catalysts (weight based) with metal nanoparticles deposited inside and alternatively outside of SMWCNTs. $PdCl_2$ (Alfa Aesar GmbH & CoKG, Germany) and $Cu(NO_3)_2{\cdot}3H_2O$ (Centrohem, Serbia) were the corresponding metal precursors and acetone or xylene were used as alternative solvents for inside and outside deposition, respectively. The applied preparation protocols were adopted from the literature with some modifications [29,30]. The filling approach is based on lower surface tension of acetone as a metals solvent, which easily fills the tube interior providing both metals within the tubes confinement. The procedure involved the ultrasonic-assisted wet coimpregnation of both precursors dissolved in acetone for 4 h, following an extended mechanical stirring for 16 h at ambient conditions. The primary removal of the solvent was performed by heating at 50 °C, followed by slow heating to 120 °C by a step of 1 °C/min and kept at this temperature for 6 h in 110 cm^3/min flow of air. Prior to use, the Pd-Cu catalyst was heat treated in N_2 flow at 200 °C for 2 h and activated by reduction in H_2 flow at 200 °C for 3 h. The prepared sample was denoted as *Pd-Cu_IN*. The procedure for the deposition of metal nanoparticles on the exterior surface of short nanotubes was based on the application of xylene as a temporary blocker of MWCNT channels. This organic solvent is immiscible with the water solution of metal precursors and it prevents them from entering the nanotube channels. The procedure included mixing of nanotubes and xylene in an ultrasonic bath for 4 h at room temperature, followed by the simultaneous addition of water solutions of both metal precursors and a commercial buffer providing pH 10. After continuous stirring for 24 h, the two-layered mixture was heat treated at 80 °C until the complete evaporation of the liquid phase. The synthesized catalyst was then subjected to static drying and additionally purified by ultrasonic treatment in order to remove the buffer remains. The heat treatment and reduction steps were performed under the same conditions as for the catalyst having metals inside the nanotube channels. The obtained catalyst was denoted as *Pd-Cu_OUT*. EDS analysis was performed in order to examine the metals present in the catalyst samples, both qualitatively and quantitatively. The results of elemental analysis indicate that both catalyst samples have both metals loading close to the nominal one, *i.e.* 0.26 at. % (2.23 wt.%) and 0.24 at.% (1.23 wt.%), for Pd and Cu, respectively for the Pd-Cu_IN sample, and 0.25 at.% (2.15 wt.%) and 0.22 at.% (1.13 wt.%), for Pd and Cu, respectively, for the Pd-Cu_OUT sample.

2.4. Test reaction – catalytic denitration

The performances of the two bimetallic Pd-Cu catalysts were tested in catalytic water denitration reaction in a semi-batch reactor equipped with magnetic stirrer [31]. The reaction was performed with 300 ml of water having initial concentration of 100 ppm NO_3^- and using catalyst loading of 100 mg. Reaction temperature was 25 °C, pressure 1 bar, and equal flows of H_2 and CO_2 of 110 cm^3/min were maintained throughout the reaction. Mixing was performed at 500 rpm and pH was controlled as 6.

The performed test reaction procedure was as follows:

The previously reduced catalyst was fed into the reactor with demineralized water under constant stirring. In order to remove dissolved oxygen, nitrogen (110 cm^3/min) was passed through the reaction mixture for 15 min, followed by the gas mixture of hydrogen and carbon-dioxide (220 cm^3/min), the last acting as a pH buffer. Following the gas saturation of the system in the first 30 min, a certain volume of $NaNO_3$ (Centrohem, Serbia) solution was added to the catalytic water suspension in order to achieve an initial NO_3^- concentration. In order to follow the denitration reaction kinetics samples were taken from the reactor for determination of nitrate, nitrite and ammonium concentrations. The content of these ions was analyzed by UV–vis spectrophotometry (Cecil Instruments 2021) with the additional use of Lovibond CheckKit reagents (Tintometer GmbH, Germany) for color change chemical reactions.

2.5. Characterization methods for MWCNT samples and related Pd-Cu catalysts

The morphology of SMWCNTs and related Pd-Cu catalysts were characterized by transmission electron microscopy (FEI TECNAI G2 20X-TWIN Transmission Electron Microscope) (TEM). The texture of the samples was investigated by means of specific surface area determined by fitting the BET isotherm equation, mean pore diameter and pore volume determined from the desorption part of the N_2 isotherm by the Barrett-Joyner-Halenda (BJH) method. Pores were classified according to Brunauer-Deming-Deming-Teller method based on hysteresis loops of adsorption-desorption isotherms [32]. Corresponding data for textural characterization were obtained by dynamic low temperature N_2 adsorption/desorption (LTNA) method, with He as a carrier gas, using a Micromeritics ASAP 2010 instrument. X-ray diffraction (XRD) measurements were performed on a Rigaku Miniflex 600 unit (Cu Kα radiation, $\lambda = 0.15406$ nm) using a counting step of 0.3° and a counting time per step of 3 s. The average diameters of crystallites were derived using the Scherrer equation. Raman spectra of the samples were obtained using a DXR Raman Microscope equipped with a diode pumped solid state laser (DPSS) with an excitation wavelength of $\lambda = 532$ nm. The laser was coupled with a CCD camera as a detector, full range grating (900 lines/mm), 10× microscope objectives and OMNIC software for collecting and analyzing the spectra. All samples were exposed to the radiation of the laser with power of 9 mW, six times for 30 s. Catalyst leaching was tested by means of ICP-MS measurements performed in an Agilent 7700× instrument. Pd-105 and Cu-63 isotopes were detected using a He collision cell to reduce spectral interference effects.

3. Results and discussion

3.1. Characterization of MWCNT samples and related Pd-Cu catalysts

As can be seen from Fig. 1a, the morphology of original long MWCNTs can be characterized as highly twisted and entangled tube structures forming a dense network. The nanotubes have external diameter mostly varying within 5–20 nm, while their lengths range from several hundred nanometers to a few micrometers (Table 1). The accurate determination of MWCNT length is quite difficult due to their specific morphology. According to the results of TEM analysis, around 80% of the starting material was successfully cut to MWCNTs fragments – the shorter open-ended tubes with lengths in the range of 100–800 nm (Fig. 1b, Table 1). The obtained relatively broad length distribution can be explained by the coexistence of both short and longer tubes, the previous bearing pits indicating the locations of the cutting process which is in progress. Consequently, the resulting cutting products are SMWCNTs and a fraction of tubes that are not completely cut (marked by arrows in Fig. 1b). Taking into account the size of these pits, it can be suggested that they might resemble the size of Ag nanoparticles previously situated here and acting as efficient catalytic centers. Thus, the formed pits are the consequence of CNT consumption by carbon oxidative etching catalyzed by Ag and can be considered as spots of the tube damaged structure in addition to tube ends. Furthermore, no structural damages were observed on the exterior walls of MWCNTs beyond their contact points with Ag nanoparticles.

Obviously, the catalytic oxidation can be very efficient method for shortening the tubes, in terms of both cutting extent and individual MWCNT length reduction. The effect is probably emphasized by the applied pre-treatment of the original long MWCNTs using nitric acid, which has preceded the oxidation. The nature and the amount of defect sites and sites with attached functional groups have already been confirmed in our previous studies [24,33]. The beneficial aspect of the present tube defects and functional groups in Ag-catalyzed cutting process has already been evoked in the literature – defects could provide oxygen *via* oxygen containing functional groups and/or improve nanoparticle-nanotube interaction [27]. The latter would enable direct contact of Ag atoms with C atoms at the nanotube surface through π-bonding, thus reducing the strength of C bonds and facilitating the oxidation [28].

The morphology and size of bimetallic Pd-Cu nanoparticles deposited on inner and exterior walls of short carbon nanotubes were also investigated by TEM and the representative images with the corresponding histograms of metal size distribution (based on the measurements of 150 nanoparticles for each sample) are shown in Figs. 2 and 3. TEM image of Pd-Cu_IN (Fig. 2a) shows that all the metal nanoparticles were homogeneously distributed inside the oxidatively cut MWCNTs. The particles have a predominant round shape exhibiting a rather narrow size distribution within the range of 1.5–8.2 nm. The presence of individual standalone particles (not attached to any part of the tubes) was not observed. In this regard, a majority of nanoparticles can be found attached to the inner tube walls. The achieved high selectivity of tube filling is usually attributed to the specific tubular morphology of the CNTs, which, in conjunction with the usage of low surface tension solvent induces the capillary forces. It has been evoked in the literature that the wide cavities are more prone to filling than the narrow ones. Namely, the small confined tube space is characterized by the presence of van der Waals repulsion forces that overwhelm the capillary ones, and thus inhibit the metal precursor penetration [34]. Some research studies have also showed that there is a correlation between the metal particle size and MWCNT inner diameter, *i.e.* the smaller particles are preferentially created in the small cavities and *vice versa* [35]. The results obtained in this study imply that particle positioning exclusively inside the narrow tubes can be successfully realized by selecting the appropriate solvent and extending the treatment time during the catalyst synthesis. However, the exact relationship between the size of metal nanoparticles and the CNT cavity diameter can not be established. The microscopy image of the Pd-Cu_OUT (Fig. 2b) shows the presence of well-defined round shaped metal nanoparticles attached to the external surface of the nanotubes. According to the corresponding histogram (Fig. 3b), this sample can be characterized by a broader particle size range (2.2–13.1 nm) than its confined counterpart. The fact that majority of the particles were dispersed on the exterior of CNTs suggests that the applied preparation procedure enabled the wetting of the tube external walls by the metal precursors after the tube cavities have been efficiently blocked by xylene. The mean diameter of the

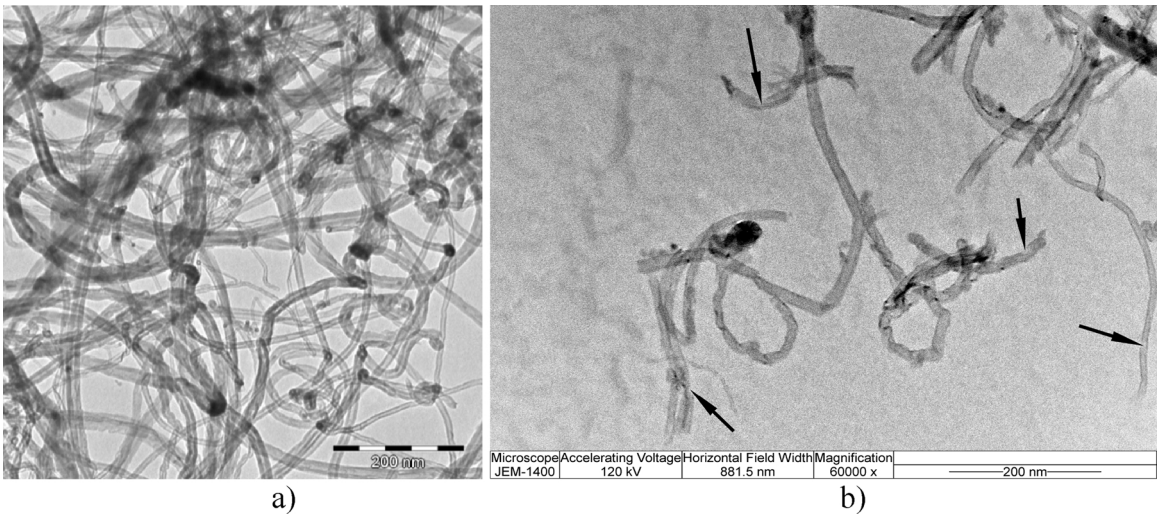

Fig. 1. TEM images of a) LMWCNTs and b) SMWCNTs.

particles located outside the CNTs (6.2 nm) was slightly larger compared to the diameter of the confined ones (4.1 nm) (Table 1). This might be interpreted as a consequence of spatial tube restrictions in terms of particle growth, but also as an indication of different metal-support interaction. The former is partly manifested through a pyramidalization effect, explaining that higher reactivity of CNT inner (concave) surface relative to the outer (convex) one is due to higher curvature of the previous [36]. Consequently, the tubes subjected to external metal decoration experienced weaker bond between metal precursors and the CNT outer surface and a growth particle evolution preceded by Ostwald ripening and/or small clusters mobility can be assumed inducing their diameter increase (Figs. 2 b, 3 b, Table 1) [37].

Results of XRD analysis of the long and oxidatively cut MWCNT samples are given in Table 1 (XRD profiles not shown). Both patterns exhibit Bragg's reflections characteristic for crystalline graphite – the most intense sharp peak at 2θ = 26° (*002*) and a broad peak around 2θ = 43° formed by the overlapping (*100*) and (*101*) signals. Prior to XRD parameter analysis, the (*002*) peak profiles were fitted using *pseudo*-Voigt function. The obtained inter-layer distance values (d_{002}) (Bragg's law) for both samples were very similar (around 0.34 nm), while the mean crystallite size along the nanotube diameter (Debye-Scherrer's equation) was slightly reduced after the cutting process (from 3.33 nm for LMWCNTs to 2.96 nm for SMWCNTs). This might indicate that the selected cutting procedure brings minor deterioration of tubes graphitization degree (order of crystallinity). Additionally, the Ag peak was not detected in the XRD pattern of SMWCNTs confirming that Ag has been completely removed by acid purification after the oxidation reaction.

The crystalline phases of the corresponding tubes upon Pd-Cu introduction are presented in Fig. 4, witnessing on metal nanoparticles location, *i.e.* either in the internal cavity, or on the external surface of the SMWCNTs. The XRD diffraction pattern of Pd-Cu_IN shows the main characteristic peaks of face-centered-cubic (fcc) crystalline Pd located at 2Θ values of 40.2° (111), 46.6° (200) and 68.2° (220) with the obtained lattice parameter (0.389 nm) close to the reported one (COD database code: 1011110, Reference code 96-101-1111). The second crystalline phase identified inside the channels of SMWCNTs can be assigned to ordered $Cu_{1.00}Pd_{1.00}$ alloy with the reflections at 2Θ values of 42.7° (110), 62.2° (200) and 78.5° (211) (COD database code: 9008813, Reference code 96-900-8814). According to the Scherrer's equation, the average crystallite sizes of Pd and the alloy were 6.0 and 7.3 nm, respectively (Table 1). The obtained values are slightly higher than the mean particle diameter determined by TEM analysis, speaking on XRD method limitation in terms of small particle verification. The particles located on the external surface of the nanotubes contain the same crystalline phases and can be portrayed as slightly larger Pd (7.8 nm) and smaller alloy (6.1 nm) species compared to the confined ones (Table 1). In the case of exterior tube decoration, the mean particle diameter value obtained by TEM is closer to the previously reported XRD results. Dispersion values calculated for catalysts having palladium and alloy species follow their pretty similar particles size (Table 1) [38].

The obtained reversed values of palladium and alloy dispersion for Pd-Cu_IN and Pd-Cu_OUT catalysts resolved by both TEM and XRD, attributed to different MSI, require an additional explanation. Namely, both diameters of tubes and metallic particles size observed do not support the tube curvature effect as a main cause for different tube surfaces reactivity [36]. Therefore, potential influence of different outer/inner surface functionality due to both purification and cutting processes was considered based on FTIR examination. As seen from Fig. 5, next to vibrational bends at 2925 cm^{-1}, 2850 cm^{-1} and 1620 cm^{-1}, characteristic for nanotube structure, stretching vibrations

Table 1
Physico-chemical properties of examined MWCNT samples and related Pd-Cu catalysts.

Characterization methods and sample properties	*TEM*		*XRD*			*LTNA*		*Raman spectroscopy*		
Sample	CNT length (μm)	Average metal particle size (nm)	Mean crystallite size (nm)	Average metal particle size (nm) (dispersion, %)		BET (m^2/g)	Total pore volume (cm^3/g)	I_D/I_G	I_{2D}/I_G	I_{2D}/I_D
				Pd	Pd-Cu alloy					
LMWCNTs	0.1–10.0		2.96			190.1	0.8	0.92	0.56	0.60
SMWCNTs	0.1–0.8		3.33			220.8	1.4	1.01	0.55	0.54
Pd-Cu_IN		4.1		6.0 (18)	7.3 (15)	210.2	1.3	1.28	0.56	0.44
Pd-Cu_OUT		6.2		7.8 (14)	6.1 (18)	224.9	1.4	0.95	0.54	0.57

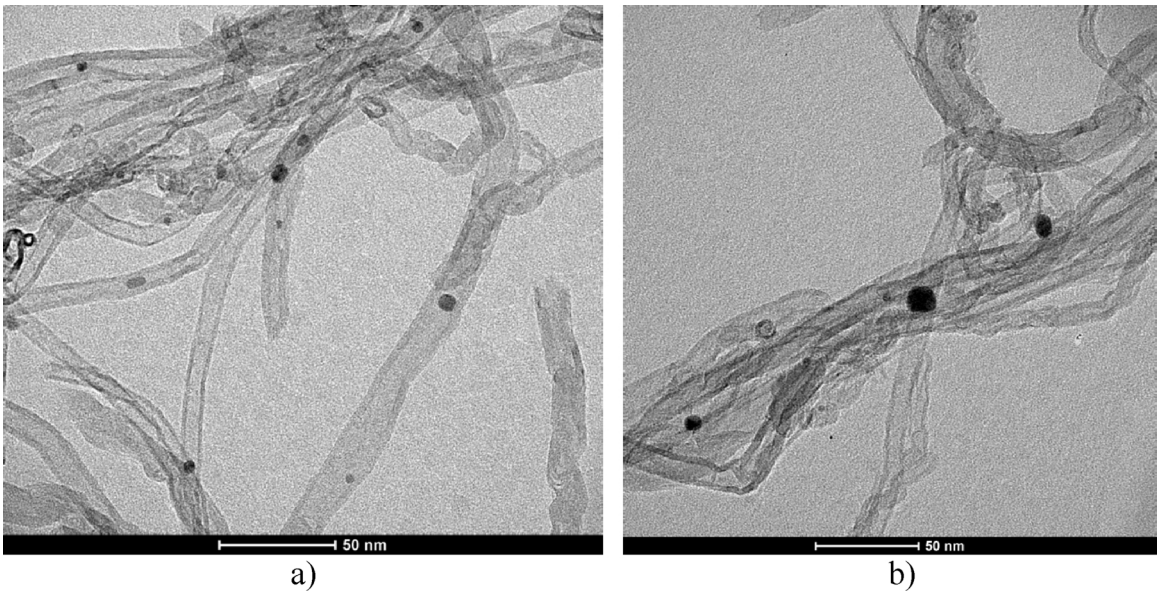

Fig. 2. TEM images of a) Pd-Cu_IN and b) Pd-Cu_OUT.

of −OH groups (3430 cm^{-1}) and carboxyl and/or carbonyl groups (1720 cm^{-1}) can be identified. The results imply that the short tubes mostly maintained a similar functionality as their long counterparts [24]. The oxygenated functional groups, sitting on tubes outer surface, are very fond of copper ion adsorption [39], resulting in stronger MSI and consequent formation of smaller external alloy particles (Table 1). In contrast, palladium does not have the same anchoring preferences towards the same functional groups [40], which makes the curvature as the main cause for the stronger MSI in the interior and consequent smaller inner palladium particles.

Textural properties of long and short MWCNT samples are given in Table 1, while N_2 adsorption–desorption isotherms and BJH pore size distributions are illustrated in Fig. 6. As expected, pore size distribution profiles (image inserted in Fig. 6) of the tubes before and after cutting are very similar due to the fact that the majority of pores in the pack of stacked intertwined nanotubes are actually made by distances between the tubes (Fig. 1a), *i.e.* interstices originating along the tangled tubes [41]. These are represented by the higher meso-range maximum in pore size distribution profiles, while the lower meso-domain, representing only a very small pore fraction attributed both to thinnest tubes interstices and inner tube channels, is visible only in the case of short MWCNTs. Availability of the short tubes openings to N_2 molecules goes along with reorganization of the tubes packing, which is portrayed by total pore volume increase in SMWCNTs relative to their long counterparts (Table 1, Fig. 1b). The presented model of the tubes organization also explains unexpected adsorption/desorption hysteresis loop H3 for both samples [32] (Fig. 6), speaking in favor of slit-shaped mesopores domination resulting from the tubes interstices, instead of cylindrical pores representing tube openings. Values for specific BET surface area show benefits of such short tubes reorganization, as there is an increase of some 15% upon the tubes cutting, the value which stays more-less constant after the active metals introduction.

Raman spectroscopy was used to assess the structural quality of the examined MWCNT samples. The corresponding Raman quality indicators were calculated as integrated intensity ratios and are given in Table 1. The spectra of both MWCNT samples (not shown) are characterized by three intense peaks around 1340 cm^{-1}, 1580 cm^{-1} and 2680 cm^{-1}, associated with the D, G and 2D bands, respectively. The common interpretations of these bands are related to the structural defects in the graphitic tube walls (D band), high symmetry of ordered MWCNTs (G band) and their crystallinity degree (2D band) [42]. Raman quality indicators revealed that original long MWCNTs have

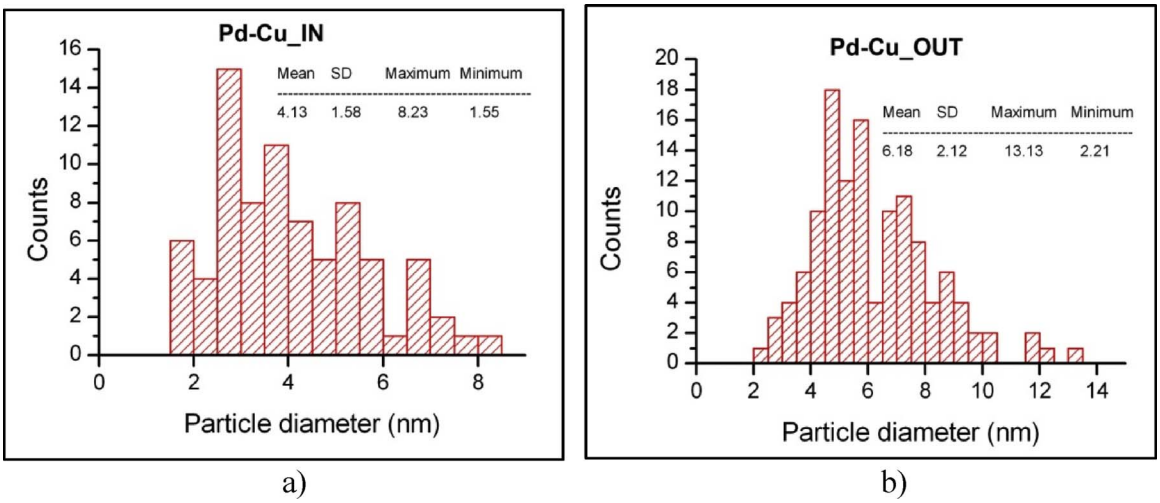

Fig. 3. Histograms of metal particle size distribution of examined Pd-Cu catalysts.

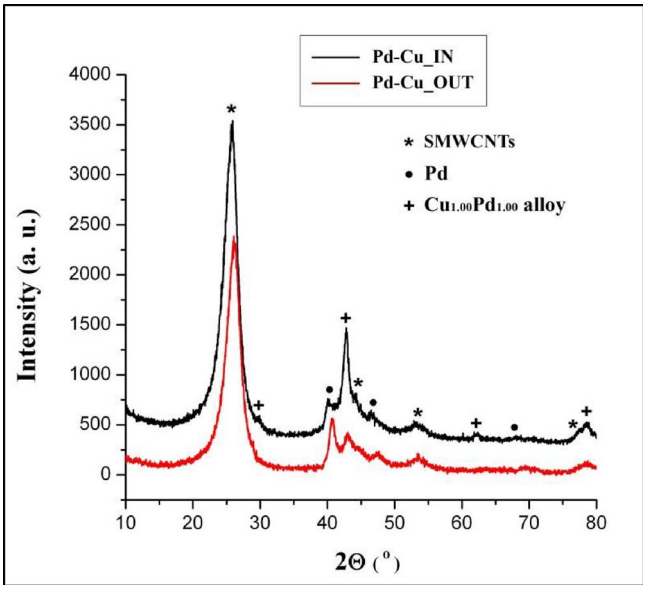

Fig. 4. The XRD patterns of examined Pd-Cu catalysts.

undergone a slight structural modification during the cutting process. Thus, the higher I_D/I_G ratio (1.01) indicates increased defects density, while the similar values of crystallinity indicators (I_{2D}/I_G, I_{2D}/I_D) imply that the multilayer graphitic structure was not significantly deteriorated. Based on this quality assessment, it can be suggested that the applied oxidation reaction using Ag nanoparticles represents a suitable method for the production of short nanotubes with almost unchanged quality and minimal introduction of structural defects.

Raman spectra of the synthesized Pd-Cu catalysts are presented in Fig. 7, while the calculated quality indicators are displayed in Table 1. Both Pd-Cu catalysts exhibit the same characteristic Raman features (D, G and 2D) as the corresponding SMWCNTs. In order to test the potential structural quality deterioration of the nanotubes imposed by the active component introduction into, or on the tube exterior walls, the comparative analysis of the Raman quality indicators was performed. As seen from Table 1, the deposition of metal nanoparticles on the outer surface of the short nanotubes has caused almost insignificant chemical changes. On the other hand, the increase of the I_D/I_G ratio upon the metal confinement treatment (I_D/I_G = 1.28) suggests the creation of new defect sites, while the approximately same value of I_{2D}/I_G ratio confirms the preservation of the tubes multilayer graphitization degree. The additional band located at 624 cm^{-1}, attributed to the vibrations of Pd−C bond at the interface between a metal and a graphitic layer [43], is more intensive in the case of the OUT sample, indicating larger single phase Pd nanocrystallites (Table 1).

3.2. Catalytic tests

Prior to catalytic tests blank experiments were performed. Over synthesized Pd-Cu catalysts but without presence of H_2 as a reducing agent no nitrate reduction capacity was observed. The activities of the tested Pd-Cu catalysts in nitrate reduction were expressed as the remaining content of nitrate ions (ppm) in the system as a function of reaction time. The degree of the nitrate ion conversion (X%) was calculated from the following expression:

$$X(NO_3^-) = \frac{n_i(NO_3^-) - n(NO_3^-)}{n_i(NO_3^-)} \cdot 100\,(\%) \quad (1)$$

where $n_i(NO_3^-)$is the initial amount of nitrate ions (mmol) and $n(NO_3^-)$is the amount of nitrate ions present at time t (mmol).

The selectivities of the tested catalysts (S%) were determined using the final quantities (mmol) of the resulting nitrogen, as the desired product, nitrite ions as intermediate, and ammonium ions, as the undesired product at reaction time t (min). The following expressions were employed for the calculation:

$$S(N_2) = \frac{2 \cdot n(N_2)}{n_i(NO_3^-) - n(NO_3^-)} \cdot 100\,(\%) \quad (2)$$

$$S(NO_2^-) = \frac{n(NO_2^-)}{n_i(NO_3^-) - n(NO_3^-)} \cdot 100\,(\%) \quad (3)$$

$$S(NH_4^+) = \frac{n(NH_4^+)}{n_i(NO_3^-) - n(NO_3^-)} \cdot 100\,(\%) \quad (4)$$

where $n_i(NO_3^-)$(mmol) and $n(NO_3^-)$(mmol) have the same meaning as in Eq. (1), while $n(N_2)$ (mmol), $n(NO_2^-)$(mmol) and $n(NH_4^+)$(mmol) are the amounts of the respective species at time t. The quantity of nitrogen was determined as a difference between the whole amount of converted nitrate ions and sum of resulted ammonia and nitrite ions, accounting for the corresponding stoichiometric ratio. The calculation assumed no other NO_X formation next toNO_2^-.

According to the widely accepted reaction scheme (Scheme 1), the

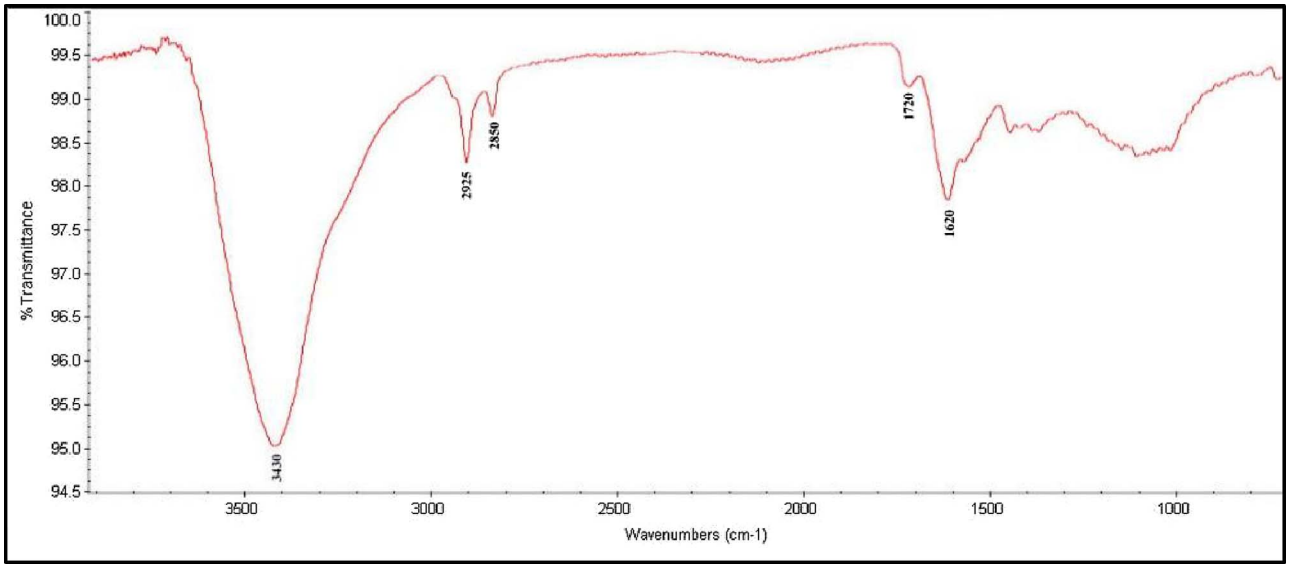

Fig. 5. FTIR spectra of SMWCNTs.

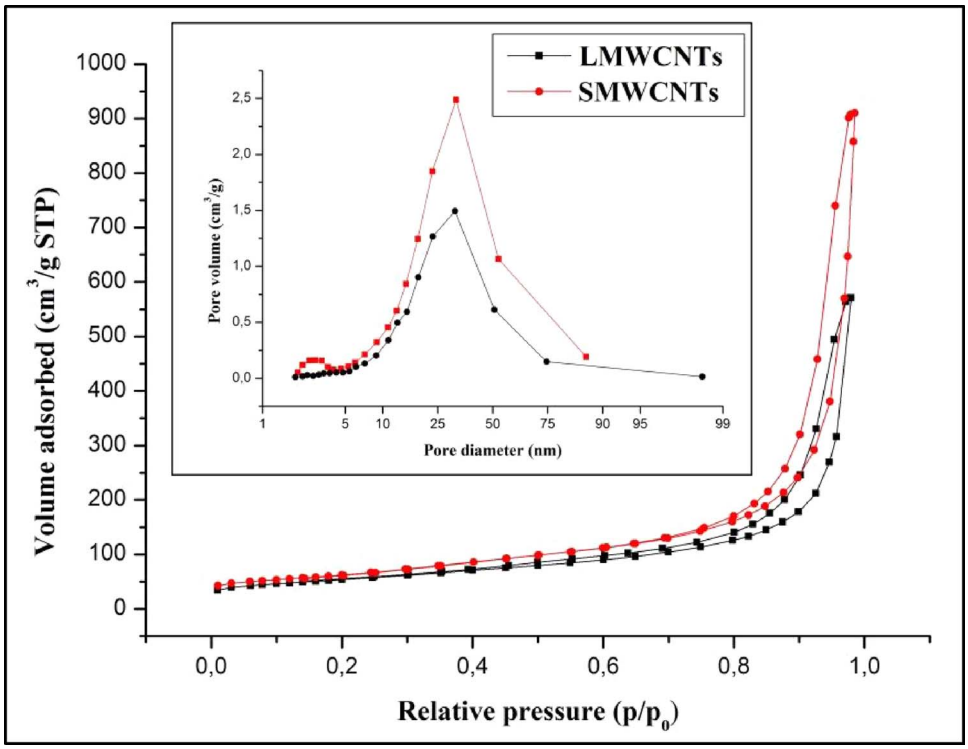

Fig. 6. N_2 adsorption–desorption isotherms of LMWCNTs and SMWCNTs with the inset of BJH pore size distribution from the desorption part of the isotherm.

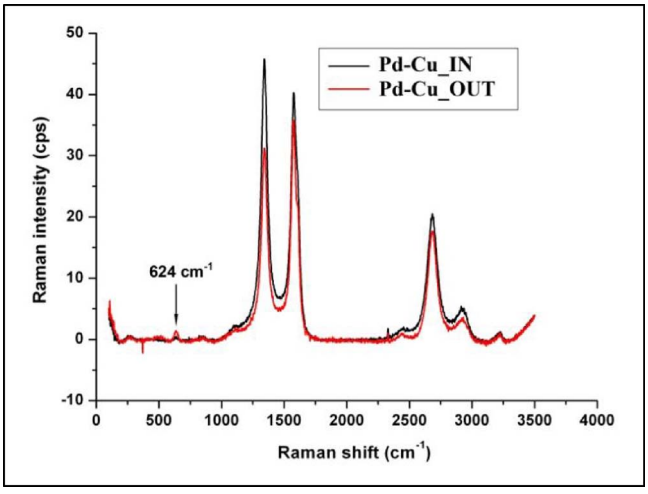

Fig. 7. Raman spectra of examined Pd-Cu catalysts.

$$NO_3^- + H_2 \xrightarrow[Pd-Cu]{k_1} NO_2^- \xrightarrow[Pd]{k_2} N_2,\ NH_4^+$$

Scheme 1. Proposed catalytic denitration mechanism.

kinetics of denitration was studied in this work assuming first-order decay for both steps in the consecutive reaction [44]:

The appropriate reaction rate equations with their integral solutions were applied:

$$-\frac{dc(NO_3^-)}{dt} = k_1 c(NO_3^-) \quad (5)$$

$$c(NO_3^-) = c_i(NO_3^-)e^{-k_1 t} \quad (6)$$

$$\frac{dc(NO_2^-)}{dt} = k_1 c_i(NO_3^-) - k_2 c(NO_2^-) \quad (7)$$

$$c(NO_2^-) = \frac{k_1 c_i(NO_3^-)}{k_2 - k_1}\left[e^{-k_1 t} - e^{-k_2 t}\right] + c_i(NO_2^-)\cdot e^{-k_2 t} \quad (8)$$

where $c_i(NO_3^-)$ and $c_i(NO_2^-)$ are initial concentrations of nitrate and nitrite ions (ppm); $c(NO_3^-)$ and $c(NO_2^-)$represent concentrations of same ion species at time t (min); k_1 and k_2 are the reaction rate constants for NO_3^- and NO_2^- conversion, respectively (calculated from the best fit of experimental data – lines in Fig. 8a and b). The influence of hydrogen partial pressure was not included in the kinetic calculations, and its value was kept constant during all the experiments. Assuming the nitrate conversion as a consecutive reaction, turnover frequency (TOF) values were calculated for both steps. However, unlike the usual approach in literature where TOF values have been determined from two separate model systems with spiked amounts of NO_3^- and NO_2^-, *i.e.* two independent reactions [45–47], in this paper related TOF values derive from one consecutive reaction (Scheme 1). Accordingly, the initial concentrations were taken only after 15 min from the reaction start in order to take into account a real (measured) concentration value of NO_2^- (Fig. 8b) and to compare catalyst efficiency for two consecutive reactions in the same time frame (285 min).

The obtained catalytic performances in time-on-stream are shown in Fig. 8, while values of nitrate conversion and appropriate selectivities, TOF, as well as reaction rate constants are summarized in Table 2.

As can be seen from the presented results, the Pd-Cu_OUT catalyst was highly active in nitrate ions removal reaching 86.9% of conversion after 300 min of reaction time, while its confined counterpart is characterized by fairly low activity of 58.8%. Both catalysts satisfy EU drinking water regulations towards maximal nitrate and nitrite concentration (50 ppm and 0.5 ppm, respectively), while the ammonium values exceeded the maximum allowable concentration (0.5 ppm) [48]. The significant difference in catalytic activities was also reflected by the reaction rate constant values for the first step of the reaction (k_1), indicating that NO_3^- were converted to NO_2^- almost two times faster over Pd-Cu_OUT relative to the Pd-Cu_IN sample (0.0053 min^{-1} *vs.* 0.0031 min^{-1}, Table 2). Both values are in the range of nitrate reduction rate constants obtained for Pt-Cu/Al_2O_3 (0.024–0.04 min^{-1}) and Pt-Cu unsupported catalysts (0.021–0.08 min^{-1}), depending on metal particle size [49]. They are also in accordance with the values of mas-

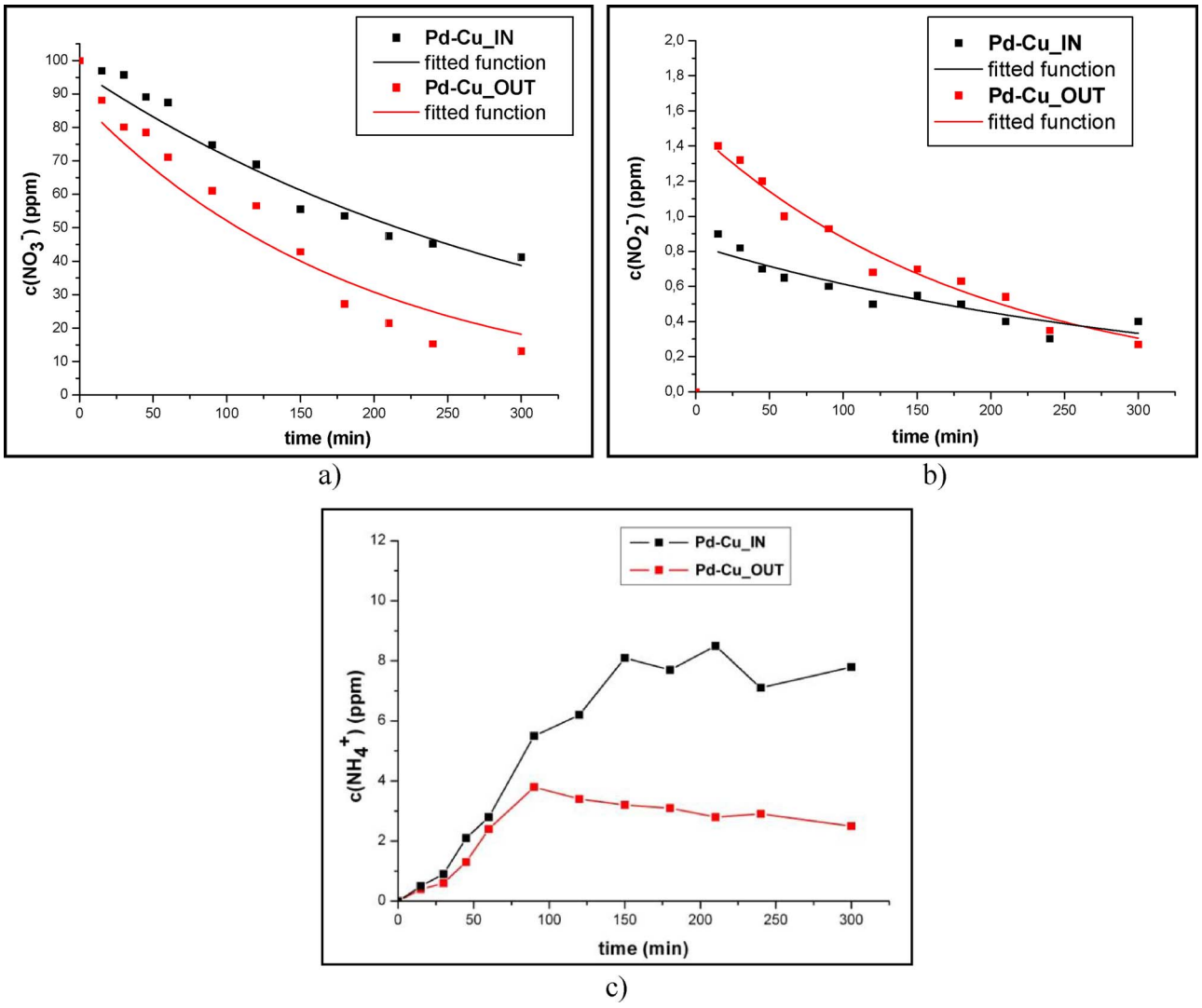

Fig. 8. Concentrations of a) nitrate; b) nitrite and c) ammonium ions as a function of reaction time during nitrate reduction in the presence of the examined Pd-Cu catalysts.

normalized pseudo-first-order rate constants, *i.e.* 0.9 l g_{Pd}^{-1} min^{-1} and 1.6 l g_{Pd}^{-1} min^{-1}, for Pd-Cu_IN and Pd-Cu_OUT catalysts, respectively, relative to 4.18 l g_{Pd}^{-1} min^{-1} for Pd-Cu on active carbon [45]. Having considered the XRD results (Fig. 4), and taking into account bimetallic Pd-Cu species as essential in the first step of the denitration process [18,19,44], it can be suggested that the nanoparticles present in the form of ordered bimetallic Pd-Cu alloy in both catalyst samples enable the production of NO_2^-. The efficiency of the Pd-Cu system can be explained by Pd pronounced effect of hydrogen spillover on Cu, enabling its regeneration and consequently the conversion of nitrate to nitrite [18,19]. The enhanced reduction of NO_3^- to NO_2^- observed in this investigation is related to smaller alloy particles located on the external walls of SMWCNTs (Table 1). The existence of an alloy might be beneficial in terms of the intimate contact between Pd and Cu, however, its catalytic performance depending on its composition and atoms arrangement [50,51]. Thus, a catalytic synergy between Pd and Cu was revealed in the case of an alloy having the Pd/Cu atomic ratio of 1:1, consequently exhibiting an optimal hydrogenation activity [52]. In the present work, the synthesized Pd-Cu alloy nanoparticles attached to the internal and external surface of the nanotubes exhibit only a slight difference in their size (7.3 nm *vs.* 6.1 nm, respectively), implying the size difference was not the main reason for the enhanced efficiency of the catalyst with exterior particles in the first reduction step. More likely it can be attributed to the specific electronic interaction between the SMWCNT surface, alloy nanoparticles and adsorbed nitrate ions. Since the interior surface of the SMWCNTs is electron-deficient [53], this reduced density can be partially compensated by the donation of electrons from the confined Pd-Cu alloy nanoparticles. On the other

Table 2
Values of nitrate conversion – X(NO_3^-), nitrite, nitrogen and ammonium selectivities – S(NO_2^-), S(N_2), S(NH_4^+), TOF and reaction rate constants, for Pd-Cu catalysts.

Sample	t = 300 min				t = 285 min			
	X (NO_3^-) (%)	S (NO_2^-) (%)	S (N_2) (%)	S (NH_4^+) (%)	TOF I step (min^{-1})	TOF II step (min^{-1})	Reaction rate constant for NO_3^- conversion, k_1 (min^{-1})	Reaction rate constant for NO_2^- conversion, k_2 (min^{-1})
Pd-Cu_IN	58.8	0.9	53.5	45.6	0.45	1.27	0.0031	0.359
Pd-Cu_OUT	86.9	0.4	89.7	9.9	0.57	2.17	0.0053	0.318

Table 3
Results of reusability test.

Reused Sample	Sequence in reusability test	X(NO_3^-) (%)	S(NO_2^-) (%)	S(N_2) (%)	S(NH_4^+) (%)	c (Pd) (ppb)	c (Cu) (ppb)
Pd-Cu_IN	1	57.4	0	47.2	52.1	2.2	35.9
	2	57.0	1.42	52.6	45.9	0.8	31.7
	3	55.0	0	49.9	50.1	1.5	63.8
Pd-Cu_OUT	1	74.5	0.5	80.5	18.9	74.2	83.4
	2	71.5	0.6	78.6	20.7	11.3	22.4
	3	69.7	0.7	79.9	19.3	9.2	23.8

hand, the externally positioned alloy nanoparticles donate fewer electrons to the support due to the electron-enriched convex surface of the nanotubes, leaving more electrons to nitrate ions as electron acceptors during their adsorption. The resulting enhanced adsorption will further facilitate the nitrate conversion. In addition, different affinity of internal and external tube surfaces towards the water model system, *i.e.* hydrophobic channels and hydrophilic external surface originating from the functionalization process (Fig. 5) may also direct the course of the reaction. Finally, the obtained lower activity of Pd-Cu_IN sample can be ascribed by the Pd-Cu nanoparticles hindrance character due to the nanoparticle and cavity size resemblance. That is to say, the larger Pd-Cu particles may act as channel blockers inducing the nitrate ions diffusion limitations (Fig. 2a). The stated results are in line with TOF values calculated for the first step of the reaction ($NO_3^- \rightarrow NO_2^-$). The higher TOF value for the Pd-Cu_OUT catalyst is due to instantaneous outer alloy particles exposure to nitrate, *i.e.* delayed NO_3^- contact with inner alloy particles due to diffusion constrains. The calculated first step TOF values for both catalysts are on the same scale as TOF values for the same Pd-Cu active phase supported on active carbon, being in the range 0.1–1.5 min^{-1} depending on the catalyst preparation method [54].

In the second reduction step (Scheme 1), the achieved TOF values are 1.27 min^{-1} and 2.17 min^{-1} for Pd-Cu_IN and Pd-Cu_OUT catalysts, respectively (Table 2). It has to be mentioned that in the applied experimental conditions of the particular consecutive reaction the second step is restricted by very low NO_2^- concentrations (Fig. 7b), especially in the case of Pd-Cu_IN catalyst sample suffering NO_3^- diffusion constrains above all. That is to say, diffusion constrains are even intensified for the same catalyst due to products (II step) and nitrate ions (I step) opposite pathways during their leaving/entering the interior of Pd-Cu_IN catalyst. As the consequence TOF ratio between two steps is higher for the OUT catalyst (3.8 *vs.* 2.8, Table 2). The same trend can be found comparing TOF values of both catalysts within the same reaction step. TOF values of the denitration reaction second step of both examined catalysts are superior to conventional ceramic based (0.06–0.21 min^{-1}) and conventional carbon based catalysts (0.04–0.24 min^{-1}) [46]. It has to be mentioned, however, that although both applied experimental approaches deal with low NO_2^- initial concentration, their different origin, *i.e.* NO_2^- as an intermediate reaction product (applied in this investigation), or NO_2^- as a starting reactant of the model system [45–47], must be considered.

The transformation of nitrite ions in the presence of nanoparticles deposited outside was governed by a slightly lower reaction rate constant (k_2 = 0.318 min^{-1}) compared to the confined sample (k_2 = 0.359 min^{-1}). These values are not far from 0.086 min^{-1} for Pt-Cu/Al_2O_3 calculated as the second step kinetics considering the consecutive reaction [49]. They are, however, up to two orders of magnitude higher from the rate constant values calculated as an individual first order decay of nitrite [55]. The fact that k_2 is two orders of magnitude higher than k_1 (Table 2), speaks in favor of the nitrate reduction as the rate-limiting step determining the rate of the overall denitration process. This is in accordance with the results of many authors claiming that the denitration reaction follows the Langmuir-Hinshelwood mechanism where the reaction between the adsorbed species (NO_3^- and H_2) can be considered as the rate determining step [18,52,56].

The significant difference in the catalytic behavior of the tested samples was also found in terms of their selectivities towards final products (N_2 and NH_4^+) (Table 2). The high concentration of ammonium ions present in the system at the end of the reaction signifies the great drawback of the Pd-Cu_IN catalyst (Fig. 7c). Consequently, the resulting selectivity to nitrogen was relatively low (53.5%). Taking into account the aforementioned mechanism (Scheme 1), it can be assumed that the substantial accumulation of ammonium ions might be due to the existence of small individual Pd nanoparticles (Fig. 4, Table 1), portrayed by higher fraction of atoms sitting on edges and corners designated as active centers for profound hydrogenation of nitrite ions into ammonium [21]. Additionally, the high ammonia selectivity may be due to higher mass transfer resistance of the ions inside the nanotubes, resulting in higher contact time furnishing deep NO_2^- hydrogenation to ammonia. On the other hand, the Pd-Cu_OUT sample can be depicted by superior selectivity towards nitrogen (Table 2). Its larger single Pd nanoparticles (Fig. 4, Table 1) also exert their geometric character by involving terraces as active centers which transform the mayor amount of nitrite ions into nitrogen [21].

3.3. Catalyst reusability

Reusability test was performed in three catalytic cycles, while catalyst leaching was followed by means of active metals concentration measured in the water model system after catalyst removal (Table 3). Catalytic runs resembled the experimental conditions of the fresh catalyst, including the catalyst thermal pretreatment in nitrogen, followed by its reduction in hydrogen. The Pd-Cu_IN sample shows pronounced durability with only small activity decrease of about 4% relative to the fresh sample after 20 h of the total working period. This is a consequence of some Cu loss, especially after the third catalytic cycle. In contrast, very low leaching of Pd might be connected to stronger MSI in the CNTs interior, leading to preserved selectivities towards both nitrogen and ammonia. As far as the Pd-Cu_OUT catalyst is concerned, its degraded activity and selectivities are due to higher leaching of both active metals (Table 3). In contrast to its counterpart, the Pd-Cu_OUT catalyst released the majority of the Pd and Cu total loss already after the first cycle. The total Pd loss is more than 20 times higher than for Pd-Cu_IN catalyst, having significant consequence on selectivity towards ammonia. It is difficult to speculate on the mechanism of Pd loss, either *via* bigger particle gradual leach, or its instant tearing from the support due to MSI weakening, the result is the same – the smaller Pd particles, favoring the ammonia production, make up most of the remaining Pd amount.

4. Conclusions

The tailoring of two carbon nanotube-based catalysts for water denitration was based on Pd-Cu active phase deposition on external and internal surfaces of short MWCNTs. The Ag-catalyzed oxidation reaction applied for cutting the originally long nanotubes was very efficient in terms of MWCNT length reduction and their structural quality preservation, including the extent of functionalization. However, the impact of the cutting procedure can be portrayed as additional tube organization with the domination of slit-shaped mesopores resulting from

the tubes interstices, instead of cylindrical pores representing tube openings, following a bonus of some 15% surface area increase. The stronger MSI, resulting in smaller both alloy particles sitting on external tube surface and palladium particles in its interior, is due to different phenomena, *i.e.* favored copper ion adsorption on numerous functional groups, in the first case, and the tube curvature following absence of the same groups, in the second. The enhanced efficiency of the catalyst with exterior particles in the first reduction step can be attributed to electron-enriched SMWCNTs convex surface, leaving more electrons to nitrate ions as electron acceptors during their adsorption and facilitating the nitrate conversion. Different affinity of internal and external tube surfaces towards water, *i.e.* hydrophobicity/hydrophilicity, and possible hindrance effect of inner channels has to be considered in terms of catalyst activity as well. The rate constant values of both steps of the consecutive denitration reaction indicate the nitrate reduction as the rate-limiting step, followed by the appropriate TOF values. As the second step (nitrite conversion) is a structure-sensitive reaction, the catalyst selectivity is primarily determined by the geometrical effect of monometallic Pd nanoparticles. That is to say, smaller Pd nanoparticles, having higher fraction of atoms sitting on edges and corners, are responsible for ammonia production. The catalyst reusability test showed lower reusable performances of Pd-Cu_OUT catalyst, which may be explained by sudden and significant leaching of both metals. The superior stability of Pd-Cu_IN catalyst can be portrayed as a total activity drop of only 4% after four consecutive runs. Thus, ambiguous location of the confined active phase in Pd-Cu_IN catalyst might find a justification when the catalyst durability is concerned.

Acknowledgements

Financial supports of Serbian Ministry of Education, Science and Technological Development [grant number 172059] is highly appreciated. Ákos Kukovecz is grateful for funding by the NKFIH (OTKA) K112531 grant. This collaborative research was partially supported by the “Széchenyi 2020” program in the framework of GINOP-2.3.2-15-2016-00013 “Intelligent materials based on functional surfaces – from syntheses to applications” project. The authors thank Albert Kéri and Gábor Galbács for the ICP-MS measurements.

References

[1] C. Pham-Huu, N. Keller, C. Estournès, G. Ehret, M.J. Ledoux, Synthesis of $CoFe_2O_4$ nanowire in carbon nanotubes. A new use of the confinement effect, Chem. Commun. (2002) 1882–1883.
[2] X. Pan, X. Bao, Reactions over catalysts confined in carbon nanotubes, Chem. Commun. 627 (2008) 6271–6281.
[3] E. Castillejos, M. Jahjah, I. Favier, A. Orejón, C. Pradel, E. Teuma, A.M. Masdeu-Bultó, P. Serp, M. Gómez, Synthesis of PtRu nanoparticles under $scCO_2$ and confinement in carbon nanotubes. Hydrogenation applications, ChemCatChem 4 (2012) 118–122.
[4] F. Zhang, F. Jiao, X. Pan, K. Gao, J. Xiao, S. Zhang, X. Bao, Tailoring the oxidation activity of Pt nanoclusters via encapsulation, ACS Catal. 5 (2015) 1381–1385.
[5] J. Zhang, S. Guo, J. Wei, Q. Xu, W. Yan, J. Fu, S. Wang, M. Cao, Z. Chen, High-efficiency encapsulation of Pt nanoparticles into the channel of carbon nanotubes as an enhanced electrocatalyst for methanol oxidation, Chem. –Eur. J. 19 (2013) 16087–16092.
[6] X. Pan, Z. Fan, W. Chen, Y. Ding, H. Luo, X. Bao, Enhanced ethanol production inside carbon-nanotube reactors containing catalytic particles, Nat. Mater. 6 (7) (2007) 507–511.
[7] S.J. Guo, X.L. Pan, H.L. Gao, Z.Q. Yang, J.J. Zhao, X.H. Bao, Probing the electronic effect of carbon nanotubes in catalysis: NH_3 synthesis with Ru nanoparticles, Chem. –Eur. J. 16 (2010) 5379–5384.
[8] J. Zhang, J.-O. Müller, W. Zheng, D. Wang, D. Su, R. Schlögl, Individual Fe-Co alloy nanoparticles on carbon nanotubes: structural and catalytic properties, Nano Lett. 8 (2008) 2738–2743.
[9] W. Zheng, J. Zhang, B. Zhu, R. Blume, Y. Zhang, K. Schlichte, R. Schlögl, F. Schüth, D.S. Su, Structure–function correlations for Ru/CNT in the catalytic decomposition of ammonia, ChemSusChem 3 (2010) 226–230.
[10] S.C. Tsang, Y.K. Chen, P.J.F. Harris, M.L.H. Green, A simple chemical method of opening and filling carbon nanotubes, Nature 372 (1994) 159–162.
[11] T.W. Ebbesen, Wetting, filling and decorating carbon nanotubes, J. Phys. Chem. Solids 57 (1996) 951–955.
[12] H.X. Ma, L.C. Wang, L.Y. Chen, C. Dong, W.C. Yu, T. Huang, Y.T. Qian, Pt nanoparticles deposited over carbon nanotubes for selective hydrogenation of cinnamaldehyde, Catal. Commun. 8 (2007) 452–456.
[13] C.F. Wang, S.J. Guo, X.L. Pan, W. Chen, X.H. Bao, Tailored cutting of carbon nanotubes and controlled dispersion of metal nanoparticles inside their channels, J. Mater. Chem. 18 (2008) 5782–5786.
[14] L.Q. Jiang, L. Gao, Modified carbon nanotubes: an effective way to selective attachment of gold nanoparticles, Carbon 41 (2003) 2923–2929.
[15] A. Aristizábal, S. Contreras, N.J. Divins, J. Llorca, F. Medina, Effect of impregnation protocol in the metallic sites of Pt–Ag/activated carbon catalysts for water denitration, Appl. Surf. Sci. 298 (2014) 75–89.
[16] L. Lemaignen, C. Tong, V. Begon, R. Burch, D. Chadwick, Catalytic denitrification of water with palladium-based catalysts supported on activated carbons, Catal. Today 75 (2002) 43–48.
[17] I. Mikami, Y. Sakamoto, Y. Yoshinaga, T. Okuhara, Kinetic and adsorption studies on the hydrogenation of nitrate and nitrite in water using Pd-Cu on active carbon support, Appl. Catal. B: Environ. 44 (2003) 79–86.
[18] A. Pintar, J. Batista, J. Levec, T. Kajiuchi, Kinetics of the catalytic liquid-phase hydrogenation of aqueous nitrate solutions, Appl. Catal. B: Environ. 11 (1996) 81–98.
[19] F. Epron, F. Gauthard, C. Pineda, J. Barbier, Catalytic reduction of nitrate and nitrite on Pt–Cu/Al_2O_3 catalysts in aqueous solution: role of the interaction between copper and platinum in the reaction, J. Catal. 198 (2001) 309–318.
[20] A. Miyazaki, K. Matsuda, F. Papa, M. Scurtu, C. Negrila, G. Dobrescu, I. Balint, Impact of particle size and metal–support interaction on denitration behavior of well-defined Pt–Cu nanoparticles, Catal. Sci. Technol. 5 (2015) 492–503.
[21] Y. Yoshinaga, T. Akita, I. Mikami, T. Okuhara, Hydrogenation of nitrate in water to nitrogen over Pd–Cu supported on active carbon, J. Catal. 207 (2002) 37–45.
[22] F. Zhang, S. Miao, Y. Yang, X. Zhang, J. Chen, N. Guan, Size-dependent hydrogenation selectivity of nitrate on Pd-Cu/TiO_2 catalysts, J. Phys. Chem. C 112 (2008) 7665–7671.
[23] S. Ratkovic, Dj. Vujicic, G. Kiss, O. Geszti, Different degrees of weak metal–support interaction in Fe–(Ni)/Al2O3 catalyst governing activity and selectivity in carbon nanotubes' production using ethylene, Mater. Chem. Phys. 129 (2011) 398–405.
[24] S. Panic, D. Rakic, V. Guzsvány, E. Kiss, G. Boskovic, Z. Kónya, Á. Kukovecz, Optimization of thiamethoxam adsorption parameters using multi-walled carbon nanotubes by means of fractional factorial design, Chemosphere 141 (2015) 87–93.
[25] A. Palermo, A. Husain, M.S. Tikhov, R.M. Lambert, Ag-catalysed epoxidation of propene and ethene: an investigation using electrochemical promotion of the effects of alkali, NO_X, and chlorine, J. Catal. 207 (2002) 331–340.
[26] A.-R. Leino, M. Mohl, J. Kukkola, P. Mäki-Arvela, T. Kokkonen, A. Shchukarev, K. Kordas, Low-temperature catalytic oxidation of multi-walled carbon nanotubes, Carbon 57 (2013) 99–107.
[27] S.A. Miners, G.A. Rance, A. La Torre, S.M. Kenny, A.N. Khlobystov, Controlled oxidative cutting of carbon nanotubes catalysed by silver nanoparticles, J. Mater. Chem. C 2 (2014) 8357–8363.
[28] A. La Torre, G.A. Rance, S.A. Miners, C. Herreros Lucas, E.F. Smith, M.W. Fay, T. Zoberbier, M.C. Giménez-López, U. Kaiser, P.D. Brown, A.N. Khlobystov, Ag-catalysed cutting of multi-walled carbon nanotubes, Nanotechnology 27 (2016) 175604–175611.
[29] Y. Gao, K. Xie, S. Mi, N. Liu, W. Huang, Preferential oxidation of CO in a H_2-rich stream over multi-walled carbon nanotubes confined Ru catalysts, Int. J. Hydrogen Energy 38 (2013) 16665–16676.
[30] Z. Guan, S. Lu, Z. Chen, C. Li, An unexpected effect of water on the asymmetric hydrogenation of α-ketoesters on platinum nanoparticles confined in carbon nanotubes, J. Catal. 305 (2013) 19–26.
[31] G. Boskovic, M. Kovacevic, E. Kiss, J. Radnik, M. Pohl, M. Schneider, U. Bentrup, A. Bruckner, Strong metal–support interaction as activity requirement of palladium supported tin oxide sol–gel catalyst for water denitration, Int. J. Environ. Sci. Technol. 9 (2012) 235–246.
[32] S. Lowell, J.E. Shields, M.A. Thomas, M. Thommes, Characterization of Porous Solids and Powders: Surface Area, Pore Size and Density, Kluwer Academic Publishers, Dordrecht/Boston/London, 2004.
[33] S. Panic, V. Guzsvány, Z. Kónya, Á. Kukovecz, G. Boskovic, Kinetic, equilibrium and thermodynamic studies of thiamethoxam adsorption by multi-walled carbon nanotubes, Int. J. Environ. Sci. Techol. 14 (2017) 1297–1306.
[34] D. Ugarte, A. Châtelain, Nanocapillarity and chemistry in carbon nanotubes, Science 274 (1996) 1897–1899.
[35] A.M. Zhang, J.L. Dong, Q.H. Xu, H.K. Rhee, X.L. Li, Palladium cluster filled in inner of carbon nanotubes and their catalytic properties in liquid phase benzene hydrogenation, Catal. Today 93–95 (2004) 347–352.
[36] Z. Chen, W. Thiel, A. Hirsch, Reactivity of the convex and concave surfaces of single-walled carbon nanotubes (SWCNTs) towards addition reactions: dependence on the carbon-atom pyramidalization, Chem. Phys. Chem. 4 (2003) 93–97.
[37] G. Boskovic, M. Baerns, Catalyst deactivation, in: M. Baerns (Ed.), Basic Principles in Applied Catalysis, Springer, Berlin, 2004, pp. 478–503.
[38] G. Bergeret, P. Gallezot, G. Ertl, H. Knözinger, J. Weitkamp (Eds.), Hanbook of Heterogeneous Catalysis, vol. 2, VCH, Weinheim, 1997, p. 441.
[39] S. Biniak, M. Pakula, G.S. Szymanski, A. Swiatkowski, Effect of activated carbon surface oxygen- and/or nitrogen-containing groups on adsorption of copper (II) ions from aqueous solution, Langmuir 15 (1999) 6117–6122.
[40] H. Kasaini, M. Goto, S. Furusaki, Selective separation of Pd(II), Rh(III) and Ru(III) ions from a mixed chloride solution using activated carbon pellets, Sep. Sci. Technol. 35 (2000) 1307–1327.
[41] G. Boskovic, S. Ratkovic, E. Kiss, O. Geszti, Carbon nanotubes purification constrains due to large Fe-Ni/Al_2O_3 catalyst particles encapsulation, Bull. Mater. Sci. 36 (2013) 1–7.

[42] L. Bokobza, J.-L. Bruneel, M. Couzi, Raman spectroscopy as a tool for the analysis of carbon-based materials (highly oriented pyrolitic graphite, multilayer graphene and multiwall carbon nanotubes) and of some of their elastomeric composites, Vib. Spectrosc. 74 (2014) 57–63.
[43] A.K. Mishra, S. Ramaprabhu, Palladium nanoparticles decorated graphite nanoplatelets for room temperature carbon dioxide adsorption, Chem. Eng. J. 187 (2012) 10–15.
[44] K.D. Vorlop, T. Tacke, Erste Schritte auf dem Weg zur edelmetallkatalysierten Nitrat- und Nitrit-Entfernung aus Trinkwasser, Chem. Ing. Technol. 61 (1989) 836–837.
[45] X. Huo, D.J. Van Hoomissen, J. Liu, S. Vyas, T.J. Strathmann, Hydrogenation of aqueous nitrate and nitrite with ruthenium catalysts, Appl. Catal. B: Environ. 211 (2017) 188–198.
[46] J.K. Chinthaginjala, L. Lefferts, Support effect on selectivity of nitrite reduction in water, Appl. Catal. B: Environ. 101 (2010) 144–149.
[47] J.K. Chinthaginjala, J.H. Bitter, L. Lefferts, Thin layer of carbon-nano-fibers (CNFs) as catalyst support for fast mass transfer in hydrogenation of nitrite, Appl. Catal. A: Gen. 383 (2010) 24–32.
[48] http://ec.europa.eu/environment/water/water-nitrates/index_en.html.
[49] A. Miyazaki, K. Matsuda, F. Papa, M. Scurtu, C. Negrila, G. Dobrescu, I. Balint, Impact of particle size and metal–support interaction on denitration behavior of well-defined Pt–Cu nanoparticles, Catal. Sci. Technol. 5 (2015) 492–503.
[50] J. Sá, S. Gross, H. Vinek, Effect of the reducing step on the properties of Pd-Cu bimetallic catalysts used for denitration, Appl. Catal. A: Gen. 294 (2005) 226–234.
[51] O.S.G.P. Soares, J.J.M. Órfão, M.F.R. Pereira, Bimetallic catalysts supported on activated carbon for the nitrate reduction in water: optimization of catalysts composition, Appl. Catal. B: Environ. 91 (2009) 441–448.
[52] F. Cai, L. Yang, S. Shan, D. Mott, B.H. Chen, J. Luo, C.-J. Zhong, Preparation of PdCu alloy nanocatalysts for nitrate hydrogenation and carbon monoxide oxidation, Catalysts 6 (2016) 96–109.
[53] Z. Peralta-Inga, P. Lane, J.S. Murray, S. Boyd, M.E. Grice, C.J. O'Connor, P. Politzer, Characterization of surface electrostatic potentials of some (5,5) and (*n*,1) carbon and boron/nitrogen model nanotubes, Nano Lett. 3 (2003) 21–28.
[54] J. Trawczyński, P. Gheek, J. Okal, M. Zawadzki, M.J. Ilan Gomez, Reduction of nitrate on active carbon supported Pd-Cu catalysts, Appl. Catal. A: Gen. 409–410 (2011) 39–47.
[55] V. Höller, K. Rådevik, I. Yuranov, L. Kiwi-Minsker, A. Renken, Reduction of nitrite-ions in water over Pd-supported on structured fibrous materials, Appl. Catal. B: Environ. 32 (2001) 143–150.
[56] J. Warna, I. Turunen, T. Salmi, T. Maunula, Kinetics of nitrate reduction in monolith reactor, Chem. Eng. Sci. 49 (1994) 5763–5773.